OPTIMISATION OF A SINGLE-PASS SUPERCONDUCTING LINAC AS A FEL DRIVER FOR THE NLS PROJECT

R. Bartolini[1,2,#], C. Christou[1], J.H. Han[1], I.P.S. Martin[1,2], J.H. Rowland[1], M.Venturini[3], D. Angal-Kalinin[4], F. Jackson[4], B. Muratori[4], P. Williams[4],

[1]Diamond Light Source, Oxfordshire, [2]John Adams Institute, University of Oxford, [3]LBNL Berkeley, CA, USA, [4]ASTeC/CI, STFC, Daresbury Laboratory, UK.

Abstract

In this paper we present the results of the optimisation of a single pass superconducting linac as a driver for the FELs of the UK's proposed New Light Source. The optimisation process requires the analysis of complicated electron beam dynamics in the presence of CSR, wakefields and space charge and has specifically taken into account the requirements for FEL operation in a seeded harmonic cascade scheme.

INTRODUCTION

The New Light Source (NLS) project was launched in April 2008 by the UK Science and Technology Facilities Council (STFC) to consider the scientific case and develop a conceptual design for a next generation light source based on a combination of advanced conventional laser and free-electron laser sources [1]. The science case for the New Light Source [2] requires the following performance from the FELs:

- photon energy range from 50 eV to 1 keV
- high brightness (>10^{11} at 1 keV)
- repetition rate ~ 1 kHz initially, increasing to 10 kHz, 100 kHz and eventually to 1 MHz
- variable polarisation
- ultra short pulses of 20 fs FWHM or less
- high degree of temporal and transverse coherence

The consultation exercise with the scientific community established that the spectral range 50 eV to 1 keV should be covered by three separate FELs whose tunability ranges are 50-300 eV, 250-850 eV and 430 eV-1 keV, respectively. Since the beginning of 2009 a significant effort has concentrated on the conceptual design of such FELs. An outline design was published in July 2009 [2] and a more extensive conceptual design will be issued at the end of 2009.

FELs based on single pass electron linacs have recently demonstrated the capability of generating high brightness FEL radiation down to the Angstrom level [3]. It appears therefore a natural choice to envisage a single pass linac driven FEL for the NLS [4]. The requirements on the repetition rate and on the temporal transverse coherence have fundamental implications on the machine type. The request for a repetition rate greater than 1 kHz rules out conventional warm linac technology. The choice adopted is a superconducting linac operating at 1.3 GHz (L-band) based on TESLA type cavities [5]. The request for a high degree of temporal coherence implies that the normal operating mode of the FEL will not be self amplified spontaneous emission (SASE) but a seeded FEL scheme has to be envisaged. Due to the lack of a powerful enough seed to cover the required spectral range, a cascaded harmonic scheme has been devised [6]. All the linac optimisation has been tailored around the optimisation of such seeded FEL scheme.

In this paper we describe the layout of the machine and the optimisation of the linac beam dynamics necessary to produce a beam with sufficient quality to drive the harmonic cascaded scheme. An initial assessment of the quality of the optimisation is performed with time dependent SASE simulations with GENESIS [7] while the final validation is made performing full start-to-end simulations of the electron dynamics from the RF gun photoinjector to the end of the undulator including the FEL dynamics in the cascaded harmonic scheme. The effect of various jitter sources in the components of the linac has been also analysed and a first assessment of the required tolerances to achieve stable FEL operation will be given.

NLS LINAC TARGETS AND LAYOUT

FELs operating in the X-ray wavelength range require very high electron beam quality with GeV energy, kA peak current and slice emittance and relative energy spread of the order of 1 μm and 10^{-4} respectively. The operation in a seeded scheme adds further constraints to the target beam quality. In fact, the requirement of a high degree of temporal coherence implies that the slice beam quality along the seed laser pulse length (20 fs FWHM) has to be as constant as possible. If significant variations in slice properties exist, the high gain FEL process will amplify them, generating again a spiky profile with poor temporal coherence. Considering a realistic linac operation including time arrival jitter sources, it is clear that the region over which the slice parameters are constant has to be long enough to accommodate not only the seed laser pulse length but also the relative timing jitter between the electron bunch and the laser seed pulse.

The choice of energy was dictated by the wavelength ranges required for the three FELs. Since the three FELs have to operate simultaneously we cannot use the linac energy for changing the wavelength since this will affect the operation of the three FEL simultaneously. The

tunability range is covered exclusively by changing the gaps of the undulators. APPLE-II devices were considered to allow the required control of the polarisation. For the long wavelength emission we decided conservatively to use magnetic gaps larger than 8 mm to limit the effect of wakefields in the undulators [8]. For the short wavelength range the gap was chosen such that the undulator parameter is larger than 0.7, since this still ensures sufficient FEL coupling and a saturation length below 50 m. These requirements can be satisfied by choosing the electron beam energy of 2.25 GeV and an undulator period of 32.2 mm [6].

Given this choice of energy and the requirements for seeded FEL operation the NLS layout was built to incorporate a photocathode RF gun, a linac with three magnetic compression stages, a beam spreader to deliver the beam to three beamlines and a train of undulators which make up the harmonic cascaded scheme.

The facility will operate in a first stage with a normal conducting L-band gun at 1 kHz repetition rate [9]. Since the beam emittance cannot be improved in the linac a careful optimisation of the beam dynamics in the space charge dominated regime has been performed achieving very good emittance and reasonable peak current.

Acceleration is achieved with a system of 14 modules of TESLA type cavities which bring the energy up to the required 2.25 GeV. At this stage a maximum gradient of 20 MV/m was considered in the simulations. However, recent investigations suggest that when the operational cost is included the optimum gradient is lowered to about 15 MV/m although the minimum is quite shallow [10]. The implications of the lower gradient operation on the linac layout have not been considered in this work and will be part of the future investigations.

The peak current of a few kA typically needed to run such FELs cannot be reached in the injector and requires a system of magnetic compression in the linac. Beam dynamics studies detailed in next paragraph have suggested that a scheme with three bunch compressors is adequate for achieving the necessary peak current while maintaining the good electron beam quality from the injector. A third harmonic cavity is introduced before the first bunch compressor to linearise the longitudinal phase space to better control the compression process along the linac. The RF gradient used in the third harmonic cavity was constrained to be lower than 15 MV/m. A laser heater is also introduced before the third harmonic cavity to control the microbunching instability. The laser wavelength was chosen to be 1030 nm and the undulator has 12 periods of 4 cm length. The required laser heater peak power to damp the microbunching instability depends on the particular compression layout and in all cases has been of the order of few MW or below.

Finally a spreader [11] is used to direct the electron beam to a set of three FELs operating in three different photon energy ranges. The electron beam spreader is based on a modified LBNL spreader design [12] with the addition of nine sextupoles for a tighter control of nonlinear effects.

A schematic layout of the facility is presented in Fig. 1. It shows the location of the RF photocathode gun (Gun), the fourteen accelerating sections (A01-A14), the bunch compressors (BC1-BC3), the laser heater (LH), the third harmonic cavity (A39), the beam spreader (SPDR) and the FEL lines.

Figure 1: Schematic layout of the NLS linac and FEL lines

BEAM DYNAMICS STUDIES

The beam dynamics in the RF photocathode gun and the first accelerating module is dominated by transverse space charge and has been optimised with Astra [13]. We will refer to the combination of RF gun and first module as the linac injector. The parameters of the optimisation were the laser spot size, the length of the flat top pulse profile, the location and strength of the solenoids, and the location of the first accelerating module. A charge of 200 pC was deemed sufficient to provide a good peak current at the end of the linac. The details of the design of the RF gun and the optimisation are reported in ref [9]. We summarise in Tab. 1 the excellent beam properties generated by the injector. The longitudinal phase space plot is reported in Fig. 2.

Table 1: beam parameters generated by the NLS injector

Energy	135 MeV
Bunch length	12 ps (rms)
Bunch charge	200 pC
Peak current	10 A
Norm. emittance proj.	0.3 μm (rms)
Norm. emittance slice	0.3 μm (rms)
Rel. energy spread slice	10^{-5}

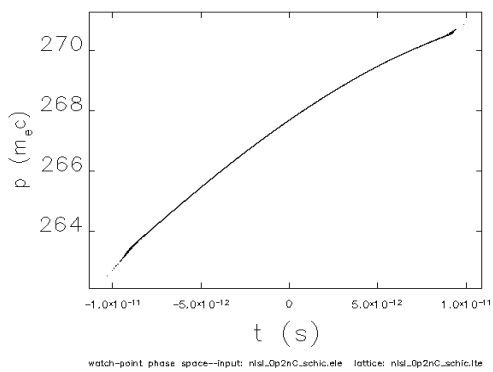

Figure 2: Longitudinal phase space at the end of the injector

Various linac layouts were considered and compared and we eventually opted for a linac with three compression stages where the last two are made of S-type chicanes, while the first one is a C-type chicane. The

linear optics of the linac was tailored to minimise the effect of CSR at the compressors by minimising the horizontal beta at the location of the last dipole. The optics functions along the whole linac, including the spreader section down to the undulator sections are shown in Fig. 3.

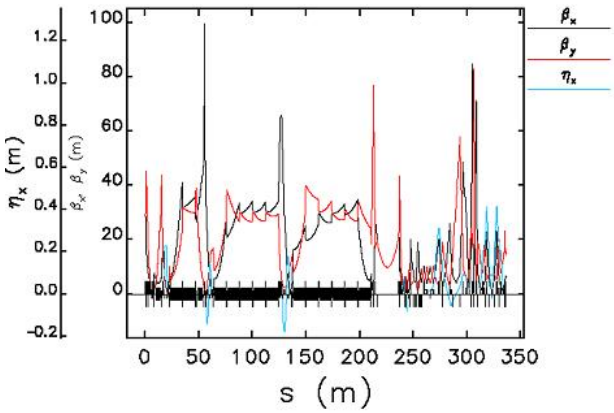

Figure 3: Optics functions for the NLS linac and spreader

Beside standard guidelines for the definition of the linear optics and the analytical setting of the harmonic cavities, we relied on numerical tracking and full start-to-end simulations to confirm the validity of the optimisation. The code elegant [14] was used to define the linac working point including the nonlinear terms in the RF, in the bunch compressors and the effects of collective effects induced by CSR, longitudinal space charge and cavity wakefields. We have devised an optimisation strategy for the linac working point, which is based on a fast evaluation of the bunch slice properties based on the Xie parameterisation of the FEL gain length [15]. The Xie parameterisation describes the effect of a realistic electron beam properties on the FEL gain length L_{3D} according to

$$L_{3D} = L_{3D}(\varepsilon_x, \sigma_\varepsilon, \sigma_x, ...)$$

In this way L_{3D} is a function of the emittance, energy spread and beam size, as well as the FEL parameters such as undulator period, field strength etc. With elegant, it is relatively fast to compute the slice properties of the beam at the beginning of the undulator and therefore relate the slice properties directly with the linac parameters used in the simulations. In this way the FEL gain length L_{3D} for each slice of the electron beam becomes a function of the linac parameters and the best slice, with the minimum gain length, can easily be selected. We also took into account that the slice parameters for the cascaded operation described in [6] have to be constant over a length which is sufficiently long to accommodate the electron beam time arrival jitter. In these studies we required constant slice properties at least over a 100 fs portion of the bunch. This was proven to be sufficient to accommodate the 20 fs laser seed pulse and the jitter in amplitude and phase of the RF cavities and in amplitude of the bunch compressors. The corresponding average gain length are functions of the RF amplitude V_k and phase φ_k of the k-th module and of the time of flight R_{56} of the three bunch compressors:

$$< L_{3D}^{best} >=< L_{3D}^{best} > (V_1, ..., V_n, \phi_1, ..., \phi_n, \theta_1, \theta_2, ...)$$

We typically used a reduced number of parameters in the linac optimisation: the phases of the accelerating sections before the first compression (including harmonic cavity); the strength of the three compressors BC1, BC2 and BC3; the phases of the accelerating sections before the second compressor. The saturation power as predicted by the Xie parameterisation was also used in the optimisation. The multi-objective multi-parameter optimiser for the analysis of the linac working point is based on a genetic algorithm with a parallel search implemented in the SPEA2 software package [16]. Fig. 4 gives an example of the result of the optimisation search performed with the optimiser. The best linac working points are at the top left of the distribution in average Xie length and saturation power.

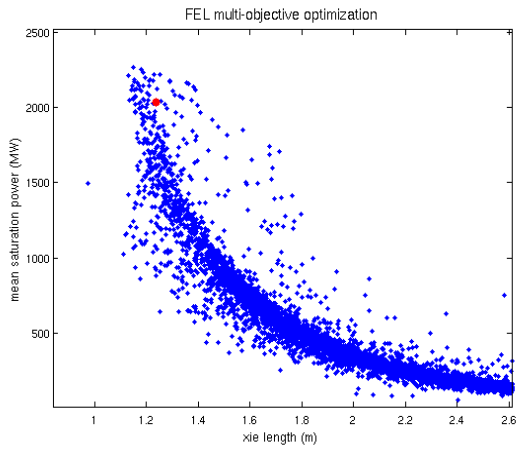

Figure 4: Example of the optimiser output. The dots on the top left correspond to linac working point with higher average saturation power and lower average 3D Xie gain length. The red dot corresponds to the best manual optimisation achieved. The improvement with the optimiser is roughly 10% in both quantities.

Many thousands of linac configurations have been explored and the best solutions were used for further final optimisation. The nominal settings for the bunch compressors and the compression factors are reported in Tab. 2. The RF voltage and phase of the main RF and the third harmonic cavity settings are summarised in Tab.3.

Table 2: Parameters of the three compression stages

	R_{56} (cm)	E (eV)	I (A)	C
BC1	-8.25	110	30	2
BC2	-11.2	440	90	3
BC3	-10.4	1260	1200	12

The analysis of the microbunching curves generated within the linear gain theory show that the microbunching gain is quite modest at all of the three bunch compressors. In Fig. 5 we report the gain curve for the first compressor where it is seen that the microbunching gain peak is only a few units.

Table 3: Parameters of the RF cavities settings

	V_{RF} (MV/m)	Phase (deg)
ACC02-03	20	10
ACC04-08	20	5
ACC08-14	20	0

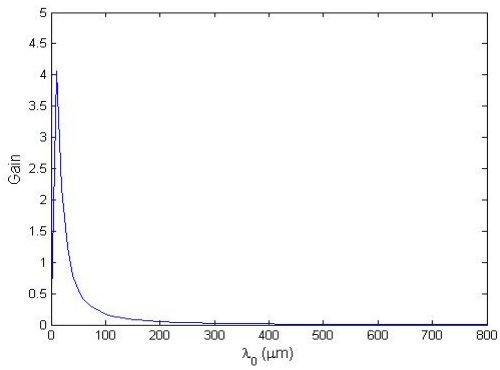

Figure 5: Microbunching gain curve at the first bunch compressor

Several beam dynamics issues have been faced in the optimisation of the linac. The layout choice was informed by the need to locate the third harmonic cavity at a sufficiently low energy to achieve an effective linearization of the longitudinal phase space with the modest gradient considered. Locating the third harmonic cavity just after the injector allows a successful linearisation of the phase space. The nominal setting to zero the quadratic curvature after the first bunch compressors has actually been exceeded during the optimisation and the curvature is overcompensated. This allows achieving a quite linear longitudinal phase space after the second bunch compressor, as the overcompensation of the quadratic chirp helps to counteract the additional curvature generated by the T_{566} at the compressors. A total gradient of 8.1 MV/m was used in the final optimisation which is well below the maximum constraint of 15 MV/m used in our optimisation

Three bunch compressions are needed to achieve the peak current required for the FEL operation. The energy of the compression, the R_{56} and the compression factor C of the three bunch compressors are reported in Tab.2. The evolution of the phase space after the three bunch compression stages is reported in Fig. 6. We opted for a distributed compression where we avoided being dominated by CSR and the LSC driven microbunching instability and also avoided strong compression at low energy in order not to be in a space charge dominated regime. The compression is roughly distributed according to the compression factors 2, 3 and 12 at the three bunch compressors respectively. The first compression stage was placed immediately after the third harmonic cavity. Given the low energy of the beam at this stage (110 MeV) the first compression is kept relatively week. The use of three bunch compressors is beneficial in redistributing the overall compression factor and relaxing the sensitivity of the bunch to various jitter sources.

In the linac optimisation we encountered noticeable difficulties in reducing the residual energy chirp imparted by the RF modules in order to compress the beam in the linac. While this issue can be tackled successfully in S-band or C-band linacs, taking advantage of the strong wakefields generated by the RF structures to compensate the residual energy chirp, this approach is not as successful in the case of L-band structures which have weaker wakefields, particularly in our case where the linac is not long enough to accumulate a significant effect. In addition, the operation with a modest charge of 200 pC, while it eases the issues related to the microbunching instabilities, prevents establishing the necessary wakefields to eliminate the residual energy chirp. Acceleration beyond crest in the last sections of the linac is also ineffective in reducing the chirp given the shortness of the bunch length with respect to the wavelength of the L-band RF. We eventually opted for a reduction of the initial chirp induced before the compression, by operating all the linac modules closer to on crest, at the expense of a stronger compression.

It turned out that the CSR in the spreader can partially compensate the residual chirp, however this effect is strongly charge dependent and intrinsically non-linear so presently it appears difficult to rely on CSR to control the residual chirp. Indeed, the microbunching instability tends to build a wedge-like structure in the longitudinal phase space if not carefully controlled which is detrimental to the beam quality.

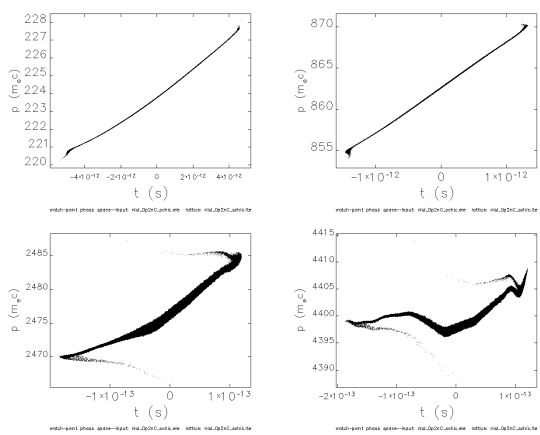

Figure 6: Longitudinal phase space at the end of the bunch compressors: BC1 (top left), BC2 (top right), BC3 (bottom left) and at the end of the spreader (bottom right)

The slice analysis of the beam at the end of the linac is described in Fig. 7 where we report the longitudinal current distribution, the normalised slice emittance, the

slice relative energy spread and the 3D Xie gain length computed for each slice. In particular, the data for the 3D Xie gain length show that the linac working point guarantees a reasonably flat region of almost 150 fs with constant slice 3D Xie length within ±10%. This condition was deemed encouraging for the linac operation of the seeded cascaded FEL and was proven sufficient to accommodate the 20 fs seed laser pulse and the linac jitter described in next paragraph.

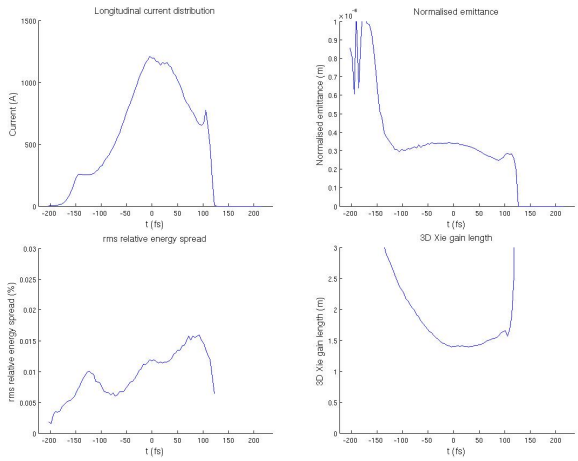

Figure 7: Slice analysis of the beam at the end of the spreader: emittance (top left), energy spread (top right), peak current (bottom left) and 3D Xie length (bottom right)

It is worthwhile to emphasise that the optimisation of the slice parameters of the beam took into account also the transverse position and angle of each slice. Indeed the FEL process was found to be significantly dependent on position offset and most of all the angle variation of the slices. The 3D Xie gain length was corrected empirically on the basis of its variation in the undulator train as per the data shown in Fig. 8.

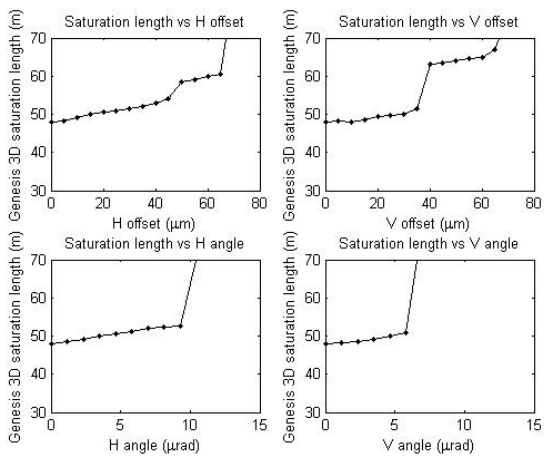

Figure 8: Dependence of the saturation length in SASE mode as a function of horizontal offset (top left), vertical offset (top right), horizontal angle (bottom left), vertical angle (bottom right).

It is seen that in an undulator train of 50 m an angular deviation of less than 10 μrad is sufficient to destroy the FEL gain. Therefore such variation in the slice parameters have been strongly penalised in the optimisation process. This criterion has had a significant impact on the bunch compressor design since it has forced us to consider a S-type chicane geometry rather than a C-type for the last two bunch compressors. The phase space plots in Fig. 9 compare the final beam in the best optimised case for the two compressor types. While the longitudinal phase space does not differ significantly, the slice offset (x, t) and the slice angle (x', t) show a significant distortion in the C-type compressors which appears to be nicely compensated in the S-type chicane compressor. We have not observed significant degradation of the beam quality due to the larger CSR power emitted in the dipoles of the S-chicane which are stronger than the C-chicane dipoles for a given R_{56}.

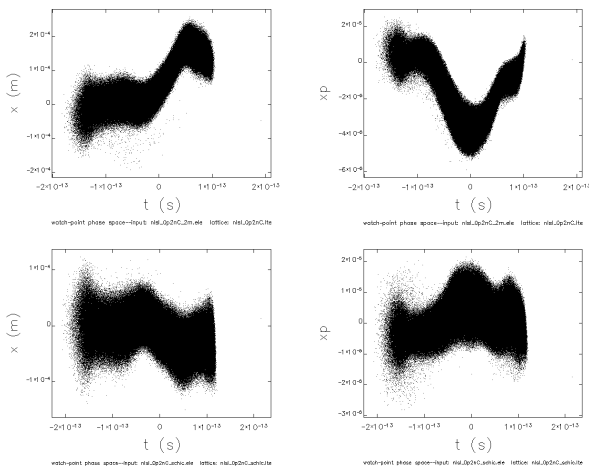

Figure 9: Phase space plots of the horizontal position (left plots) and horizontal angle (right plots) as a function of the longitudinal coordinate in the bunch: C-type chicanes (top plots) S-type chicanes (bottom plots). Notice the different scales.

The bunch obtained with the linac setting summarised in Tab. 2 ands 3 provides a beam with very good slice qualities. Time dependent SASE simulations were used to benchmark the performance of such an electron beam. Fig. 10 shows that saturation is reached within 40 m with a power of about 1.5 GW. Further FEL studies show that the slice parameters are sufficiently constant to generate a temporally coherent pulse in the seeded harmonic cascaded FEL. A time-bandwidth product of about 1 and a contrast ratio of about 40 were achieved [6].

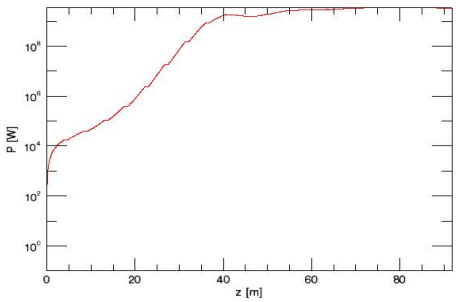

Figure 10: FEL SASE power as a function of distance along the undulator train

JITTER STUDIES

Extensive simulations were performed to investigate the effect of various jitter sources in the operation of the linac and to assess the tolerances required on the various subsystems.

The jitter sources considered in our study include both the operation of the injector and of the main linac. In particular the injector simulations include RF gun phase and voltage errors, solenoid power supply, laser intensity and position jitter [17]. In the main linac we included jitter in amplitude and phase of the RF modules and power supply ripple in the bunch compressors. A summary of the jitter amplitudes used in the initial simulations is given in Tab. 4. Simulations with Astra and elegant were coupled together to produce the final jitter as a function of the values used in Tab. 4.

Table 4: Jitter amplitudes (rms) used in the initial simulations

RF gun phase	0.1 deg
RF gun voltage	10^{-3}
Gun solenoid ps	$5{\cdot}10^{-5}$
Main RF cavity phase	0.01 deg
Main RF cavity voltage	10^{-4}
BCs power supplies	$5{\cdot}10^{-5}$

The jitter sensitivity was evaluated considering a number of physical quantities describing the electron beam at the end of the linac such as energy, slice emittance, slice energy spread and 3D Xie gain length. Particular attention was given to the arrival time jitter of the bunch, since this impacts directly on the required length of the good beam region with constant 3D Xie gain length.

A first scan of the contributions of the jitter coming from voltage and phase variations in individual linac modules was carried out. Figs. 11 and 12 report the case of the sensitivity of arrival time and final energy, respectively.

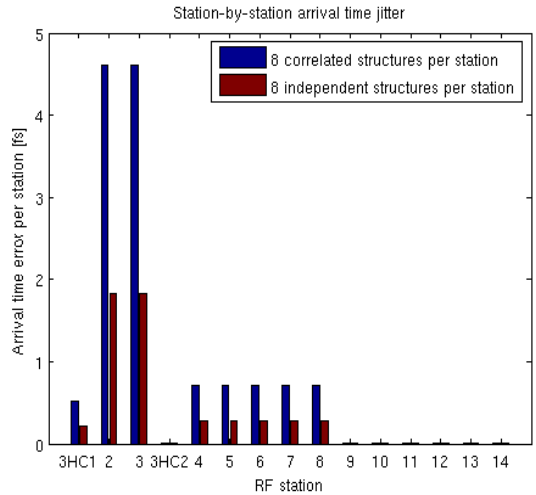

Figure 11: Arrival time jitter sensitivity module by module in amplitude and phase of the RF module of the linac

These studies pointed out that the contribution to jitter is more significant from the modules in the initial part of the linac, while after the third bunch compressors they are practically negligible. Furthermore we observed that a split in the RF distribution for the TESLA modules, where each of the eight cavities is fed independently, significantly reduces the impact of the jitter. This solution was then adopted for all the subsequent jitter studies.

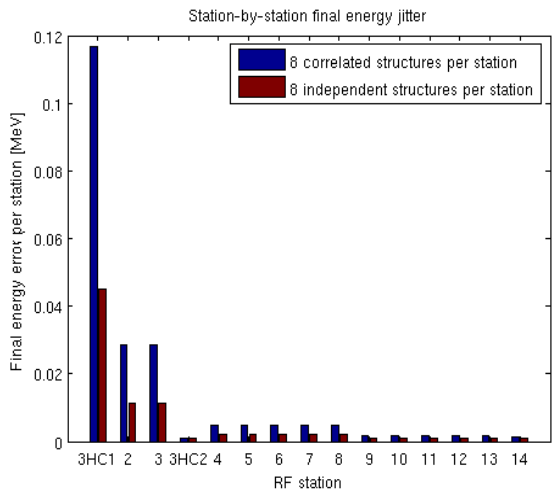

Figure 12: Energy jitter sensitivity module by module in amplitude and phase of the RF module of the linac

Starting from the nominal configuration, statistical runs were performed adding random Gaussian errors with the rms values given in Tab. 4. The power supplies of the bunch compressors are powered in series to avoid excessive transverse position jitter due to a non perfect closure of the trajectory bump. The RF distribution was split in the eight cavities of the linac modules but not in the injector. The results obtained for the rms arrival time jitter at the end of the linac are summarised in Tab. 5.

Table 5: Arrival time jitter (rms) arising from various error sources; P=phase, V=voltage, B=bunch compressor power supplies, I=injector

RF gun (P and V)	7 fs
Injector (RG Gun + ACC01)	21 fs
Main linac RF (P)	3 fs
Main linac RF (V)	9 fs
BCs power supplies	20 fs
P + V + B combined	20 fs
P + V + B + I combined	30 fs

For the jitter in arrival time we observe that the dominant effect is due to the injector (21 fs) and in particular to the first accelerating module whose eight RF cavities were fed in two independent groups instead of eight as for the other linac modules. The second largest contributor is jitter in the power supplies in the bunch compressors (20 fs) which add up roughly in quadrature with the injector jitter to make up the total arrival time jitter (30 fs rms).

A graphical view of the time jitter effect can be obtained by plotting the longitudinal current distribution and the corresponding slice 3D Xie gain length as reported in Fig. 13. It is clear that in these conditions the region of constant slice parameters necessary to accommodate the laser seed pulse is not sufficiently long and many laser seed pulses are likely to find a portion of the electron beam with non uniform slice parameters.

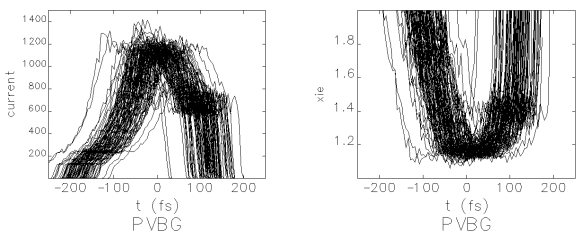

Figure 13: Current distribution (left) and slice 3D gain length for 100 jitter seeds including the whole injector and linac. No split is applied to the RF cavities of the injector module

Following the indication of Fig. 13 and Tab. 5 we have repeated the jitter studies targeting the main contribution to the arrival time jitter. We have assumed that also the cavities in the injector module are powered by independent RF sources and the relative power supply jitter in the bunch compressor has been reduced to 10^{-5}. The corresponding results for the arrival time jitter are shown in Tab. 6.

Table 6: Arrival time jitter (rms) with RF split in ACC01 and reduced jitter in bunch compressor power supplies.

RF gun (P and V)	7 fs
Injector (RG Gun + ACC01)	11 fs
Main linac RF P	3 fs
Main linac RF V	9 fs
BCs power supplies	4 fs
P + V + B combined	10 fs
P + V + B + I combined	14 fs

The beneficial effect of the RF split, and of the reduction in bunch compressor power supply jitter, is clearly put into evidence. The injector jitter is reduced to 11 fs rms and the total jitter to 14 fs rms.

The current distributions and the 3D Xie gain length in this case are plotted in Fig. 14.

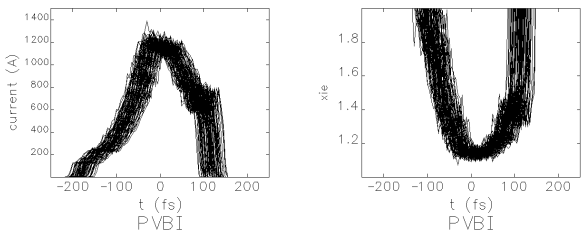

Figure 14: As Fig. 13 with the RF distribution split in each of the cavities of the first module and with reduced bunch compressor power supply jitter.

The bottom right plot in Fig. 14 shows that there exists a safe area of about 20 fs where the seed laser pulse can be fired and it is guaranteed to find a region of constant 3D Xie gain length, without being disrupted by inhomogeneities present in the electron bunch.

A bunch with similar properties has been used in the FEL simulation of the full cascade harmonic scheme in [6] showing very promising temporal characteristics.

CONCLUSIONS

We have presented a design of the linac which can deliver an electron beam of sufficiently good quality to drive a FEL at 1 keV using a seeded harmonic cascade approach. The results are supported by numerical simulations including extensive jitter studies. It is shown that modest improvement on the presently achievable technology is sufficient to achieve the requested tolerances.

Other operating working points are under consideration with lower charge to achieve shorter electron pulses to generate short (~ fs) single spike, temporally coherent, pulses. First investigations [18] show that the present layout is sufficiently flexible to produce beam quality equally suitable for these operating modes.

ACKNOWLEDGEMENTS

We would like to thank other members of the NLS Physics and Parameter Working Group and FEL Working Group, and the members of the NLS Technical Advisory Committee (chair J. Rossbach) who provided valuable feedback on the studies presented in this paper. Several discussions with A. Zholents (LBNL) are also acknowledged.

REFERENCES

[1] R.P. Walker et al., to appear in PAC09 proceedings
[2] See www.newlightsource.org for more information about the NLS project including the Science Case and Outline Facility Design.
[3] P. Emma et al., to appear in PAC09 proceedings.
[4] R Bartolini et al., to appear in PAC09 proceedings.
[5] D. Proch, TESLA Note 1994-13, (1994).
[6] N. Thompson et al., these proceedings.
[7] S. Reiche, Nucl. Inst. And Meth. **A429**, 243, (1999), and http://pbpl.physics.ucla.edu/~reiche/
[8] J. Clarke et al., these proceedings.
[9] J-H Han et al., to appear in PAC09 proceedings.
[10] P. McIntosh, private communication.
[11] F. Jackson et al., these proceedings.
[12] A. Zholents et al., CBP Tech Note 401, (2009).
[13] K. Floettmann, A Space Charge Tracking Algorithm (ASTRA), http://www.desy.de/~mpyflo.
[14] M. Borland, APS LS-287, (2000).
[15] M. Xie, in PAC95, 183, (1995).
[16] E. Zitzler et al., ETH Technical Report 103, (2001).
[17] J.H. Han et al., these proceedings.
[18] R. Bartolini et al., these proceedings.